**Photoluminescence spectroscopy of dibenzopentacene single-crystals: Multiple emissive states across temperature, time, and magnetic field in a pursuit of exothermic singlet fission**

Marco Rosenkranz, Lukas Graf, Bernd Büchner, Martin Knupfer, Alexey A. Popov*

*Leibniz Institute for Solid State and Materials Research (Leibniz-IFW Dresden), 01069 Dresden, Germany*

## Supporting Information
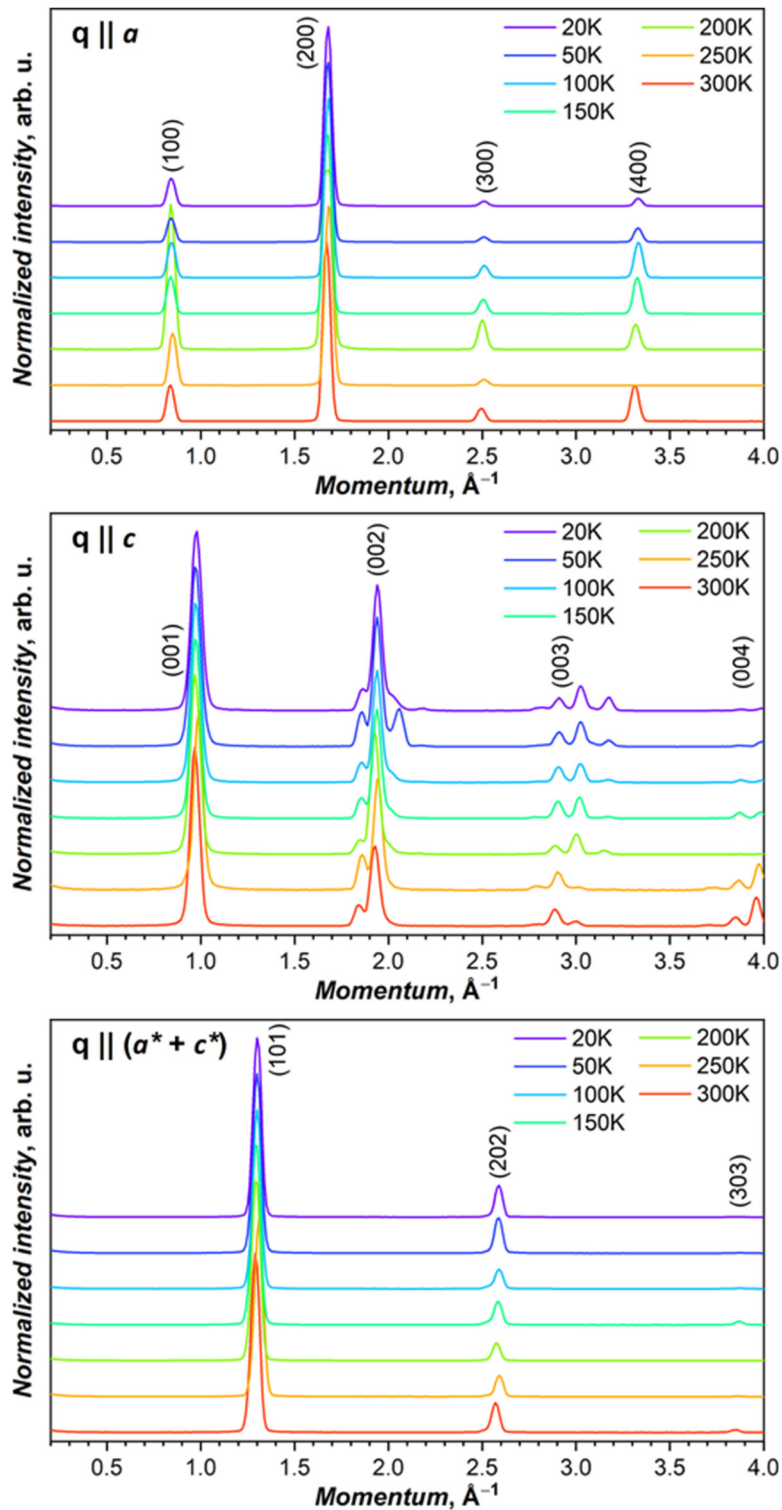
**Figure S1.** Variable-temperature electron diffraction of DBP single-crystal. The measurements were performed in EELS spectrometer, the crystal was attached to TEM Cu-grid. There are no considerable changes in diffraction patterns in *a* and diagonal (*a/c*) directions in the whole temperature range. In *c*-direction, the crystal was slightly tilted, resulting in additional peaks.
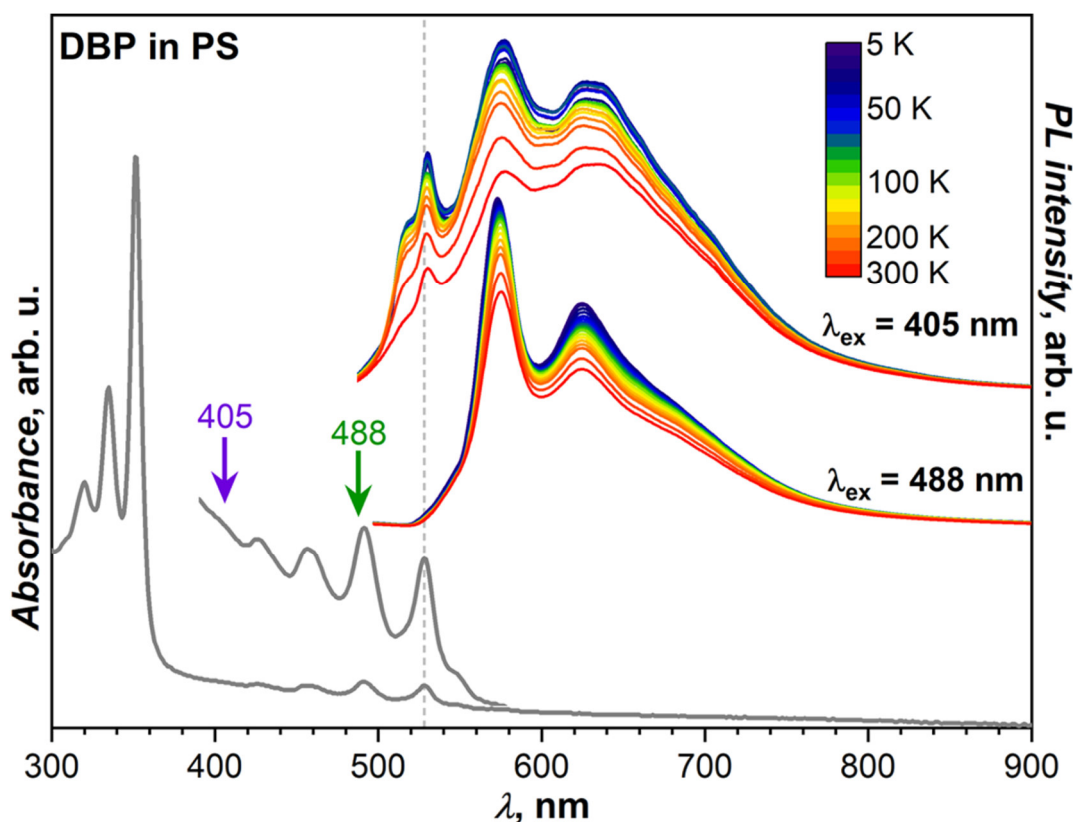
**Figure S2.** Absorption (gray line, 300 K) and emission (colored lines, different temperatures between 5 and 300 K) spectra of DBP in polystyrene matrix. PL was excited with 405 and 488 nm lasers and measured through 450 nm or 520 nm bandpass filters, respectively. 488 nm matches absorption peak of DBP and gives PL spectrum of higher quality, but the first emission peak (0–0) is cut by the 520 nm filter. For 405 nm excitation, we used 450 nm bandpass filter, and the 0–0 peak is well seen. However, the PL spectrum is overlaid with a broad parasitic signal.

Absorption peaks of DBP in PS at 528 nm/2.34 eV (0–0), 491 nm/2.53 eV (0–1), 457 nm/2.71 eV (0–2), and 426 nm/2.91 V (0–3) are close to peak positions in solution spectra. Likewise, PL peaks are seen at 532 nm/2.33 eV (0–0), 576 nm/2.15 eV (0–1), and 627 nm/1.98 eV (0–2). Vibrational energy shift of 0.18 eV is typical for PAHs and corresponds to the stretching modes of aromatic core. The Stokes shift is small: at 300 K, 0–0 absorption and emission peaks occur at 528 and 532 nm, respectively. Different from the PL spectra of the crystal, PL spectra of DBP in PS do not show strong temperature dependence. PL decay is single-exponential with time constants of 4.7±0.1 ns at 5 K and 4.2±0.1 ns at 300 K.
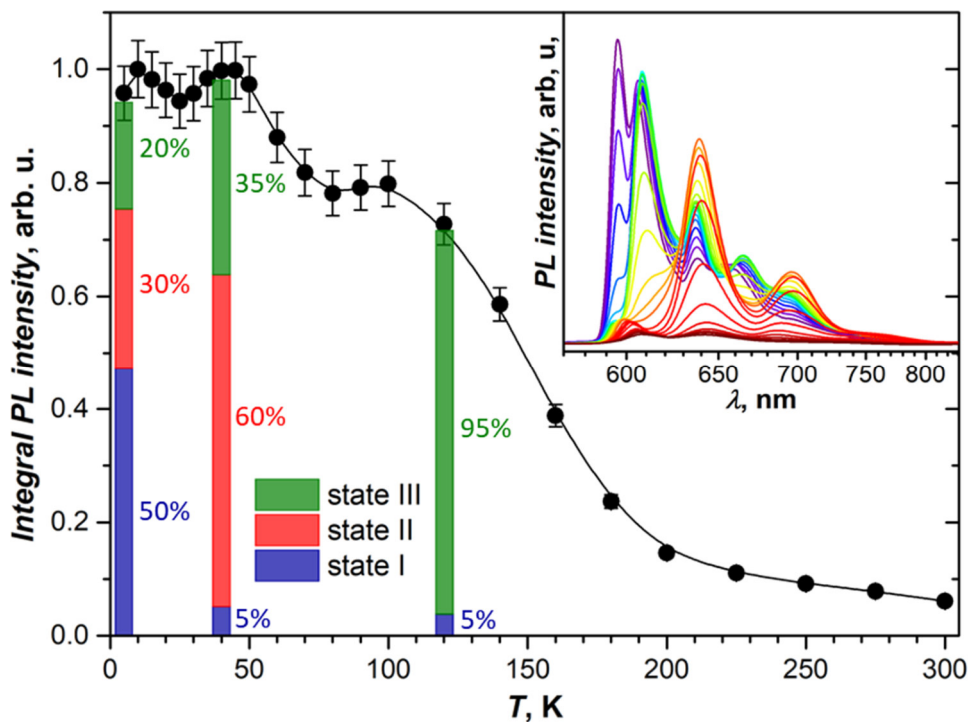
**Figure S3a.** Temperature dependence of the integral PL intensity of DBP single-crystal (PL spectra are shown in the inset). Possible uncertainty caused by defocusing and integration errors is estimated as 5% and shown as error bars. Histograms show estimated contributions of emissive states I, II, and III to the integral PL intensity at 5 K, 40 K, and 120 K.



**Figure S3b.** Variation of 0-0 peak maxima of states I, II, and III with temperature. Note that between 30 and 50 K, the peak of state I is seen as a shoulder, which may affect its determined position.

**Time-resolved measurements**



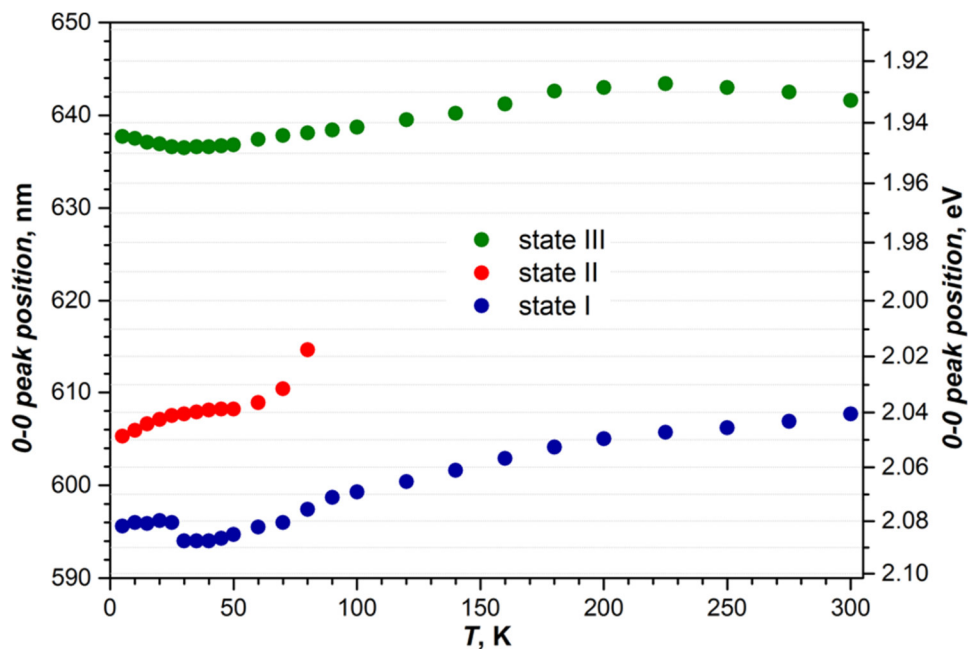**Figure S4a.** TR-PL measurements at 5 K. **(a)** PL decay curves presented as (λ, τ) maps (the same as in the main text, Fig. 3c). **(b-d)** TR-PL spectra obtained by integration of PL decay curves over indicated time interval at each recorded wavelength (step 10 nm): **(b)** stacked spectra with an offset shown in the actual relative intensity; **(c)** stacked spectra with an offset with normalized intensity in each curve; **(d)** the same as (c) but all spectra overlaid; the spectrum integrated from 66 to 146 ns is not shown in (d) because of the large noise level. Color scale and integration intervals shown in (c) are the same for (b–d).

**Figure S4b.** TR-PL measurements at 40 K. **(a)** PL decay curves presented as (λ, τ) maps (the same as in the main text, Fig. 3d). **(b-d)** TR-PL spectra obtained by integration of PL decay curves over indicated time interval at each recorded wavelength (step 10 nm): **(b)** stacked spectra with an offset shown in the actual relative intensity; **(c)** stacked spectra with an offset with normalized intensity in each curve; **(d)** the same as (c) but all spectra overlaid; the spectrum integrated from 66 to 146 ns is not shown in (d) because of the large noise level. Color scale and integration intervals shown in (c) are the same for (b–d).
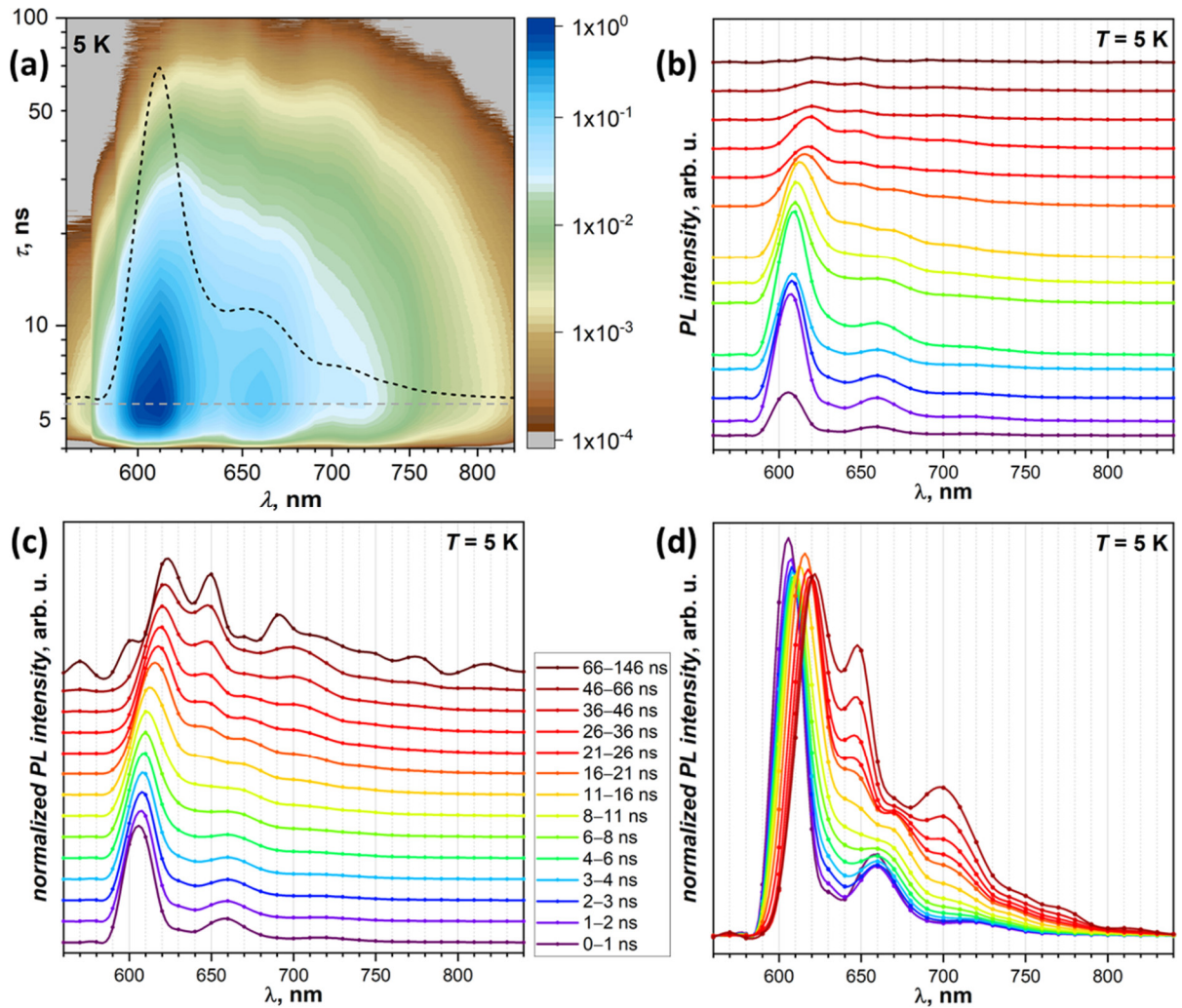
**Figure S4c.** TR-PL measurements at 140 K. **(a)** PL decay curves presented as (λ, τ) maps (the same as in the main text, Fig. 3e). **(b-d)** TR-PL spectra obtained by integration of PL decay curves over indicated time interval at each recorded wavelength (step 10 nm): **(b)** stacked spectra with an offset shown in the actual relative intensity; **(c)** stacked spectra with an offset with normalized intensity in each curve; **(d)** the same as (c) but all spectra overlaid; the spectrum integrated from 66 to 166 ns is not shown in (d) because of the large noise level. Color scale and integration intervals shown in (c) are the same for (b–d).
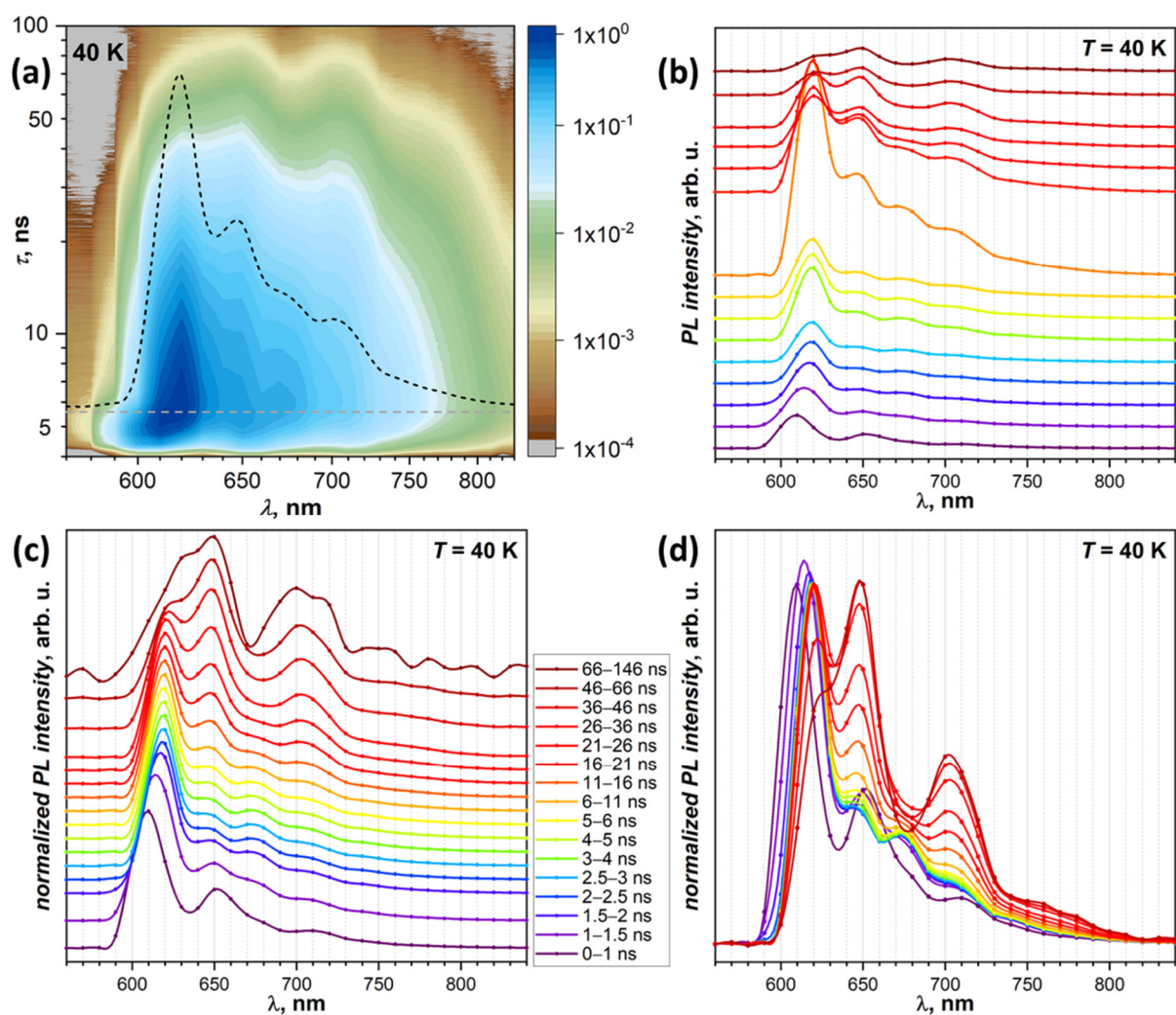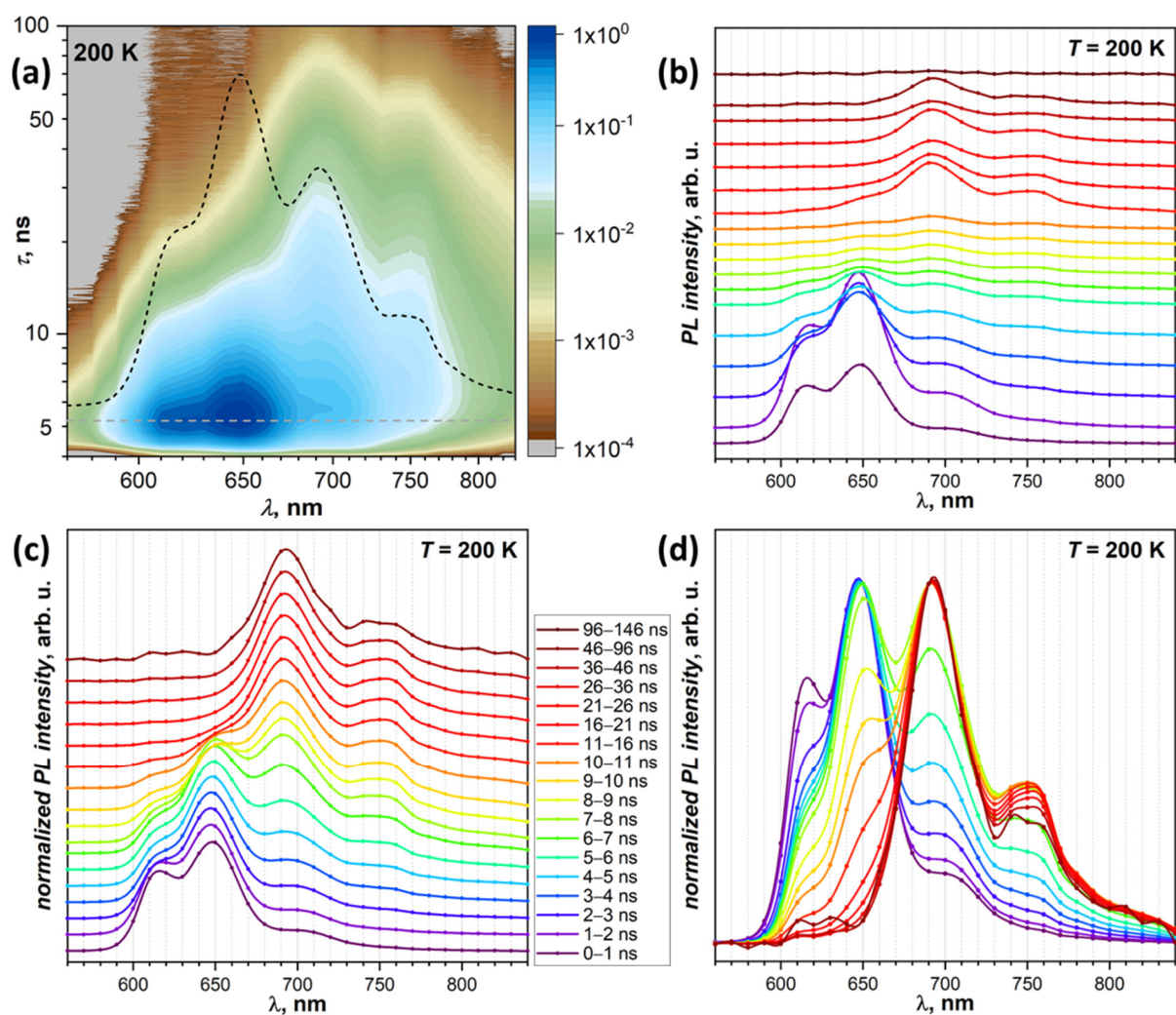
**Figure S4d.** TR-PL measurements at 200 K. **(a)** PL decay curves presented as (λ, τ) maps (the same as in the main text, Fig. 4b). **(b-d)** TR-PL spectra obtained by integration of PL decay curves over indicated time interval at each recorded wavelength (step 10 nm): **(b)** stacked spectra with an offset shown in the actual relative intensity; **(c)** stacked spectra with an offset with normalized intensity in each curve; **(d)** the same as (c) but all spectra overlaid; the spectrum integrated from 96 to 146 ns is not shown in (d) because of the high noise level. Color scale and integration intervals shown in (c) are the same for (b–d).
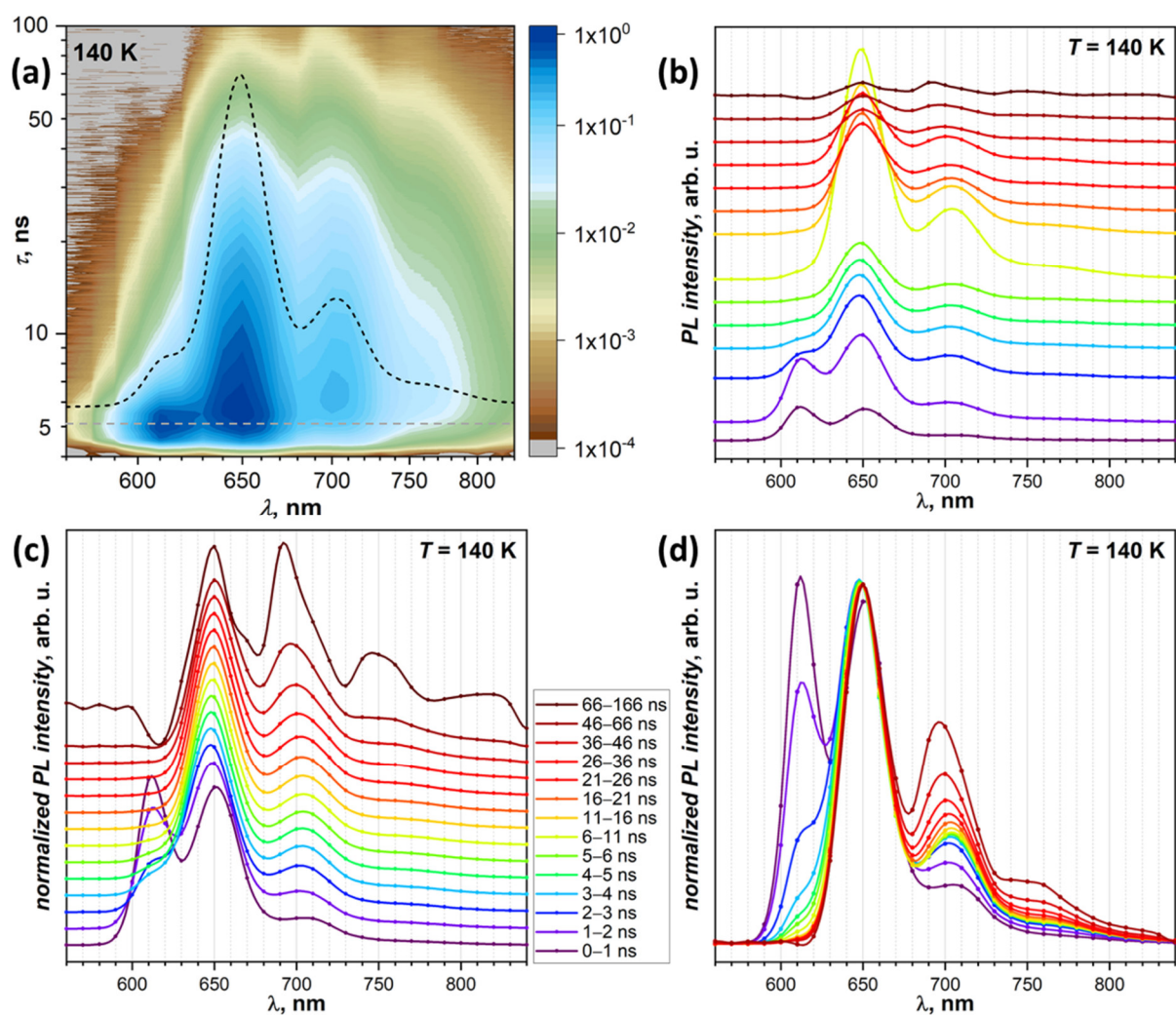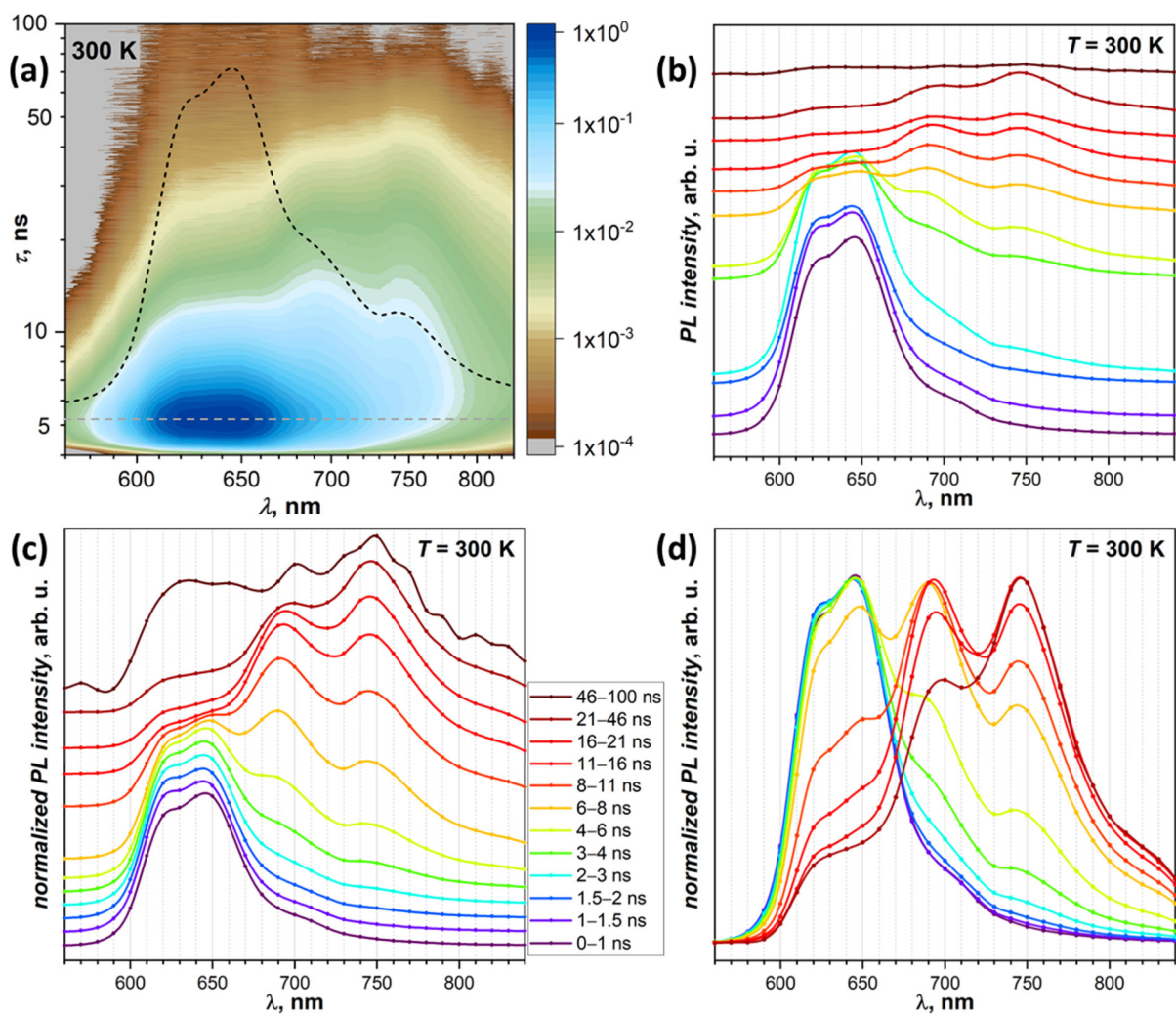
**Figure S4e.** TR-PL measurements at 300 K. **(a)** PL decay curves presented as (λ, τ) maps (the same as in the main text, Fig. 4c). **(b-d)** TR-PL spectra obtained by integration of PL decay curves over indicated time interval at each recorded wavelength (step 10 nm): **(b)** stacked spectra with an offset shown in the actual relative intensity; **(c)** stacked spectra with an offset with normalized intensity in each curve; **(d)** the same as (c) but all spectra overlaid; the spectrum integrated from 46 to 100 ns is not shown in (d) because of the large noise level. Color scale and integration intervals shown in (c) are the same for (b–d).
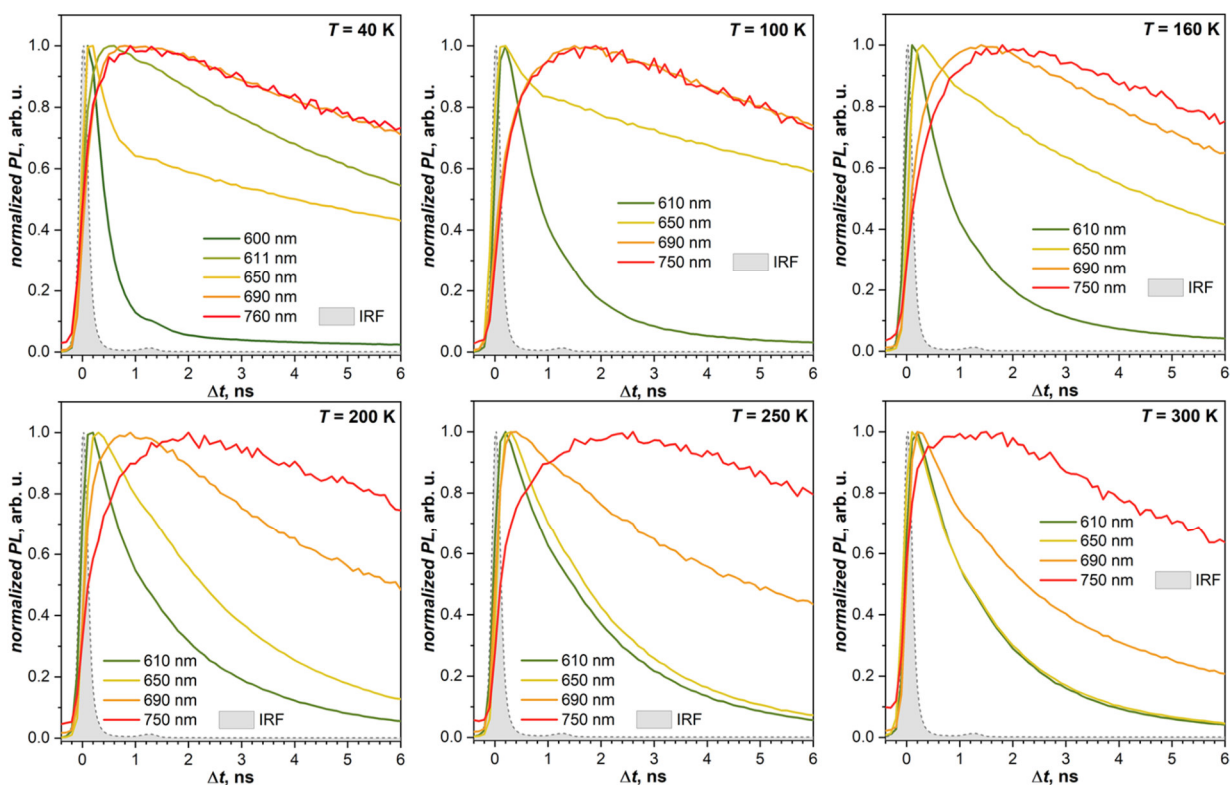
**Figure S5.** PL decay traces in the first 6 ns after laser pulse. Gray filled peak is IRF, $\Delta t = 0$ correspond to the maximum of the IRF peak. Note that the maximum of the trace at 600–610 nm (state I) occurs at 0.1–0.2 ns, state II appears slightly slower and has a maximum ca 0.1–0.2 ns after state I. This is close to time resolution of our system, so more precise rise kinetics cannot be evaluated.

The 0–0 peak of state III near 650 nm overlaps with the first vibronic feature of state I, which prevents evaluation of the early kinetics of state III. However, it can be well seen that rise/decay curve for state III becomes closer and closer to that of state I with increasing temperature, and the two curves finally merge at 300 K.

PL at 690 nm (state IV) and 750–760 nm has obviously longer risetime and reach the maximum only at ~1.5 ns after the pulse; at 40 K, rise/decay curves at both wavelengths nearly coincide. With rising temperature, the 690 nm risetime gradually shortens, along with the decrease of the state IV lifetime, while the rise time of PL at 750–760 nm remains near 1.5 ns till 250 K, and only the temperature rise above 250 K starts to shorten the risetime at 750 nm as well.

**Figure S6a.** PL decay profiles measured at different temperatures at 600–615 nm.

**Figure S6b.** PL decay profiles measured at different temperatures and wavelengths.

**Table S1a.** Multiexponential fitting of PL decay curves at 600–610 nm (dominant state I)

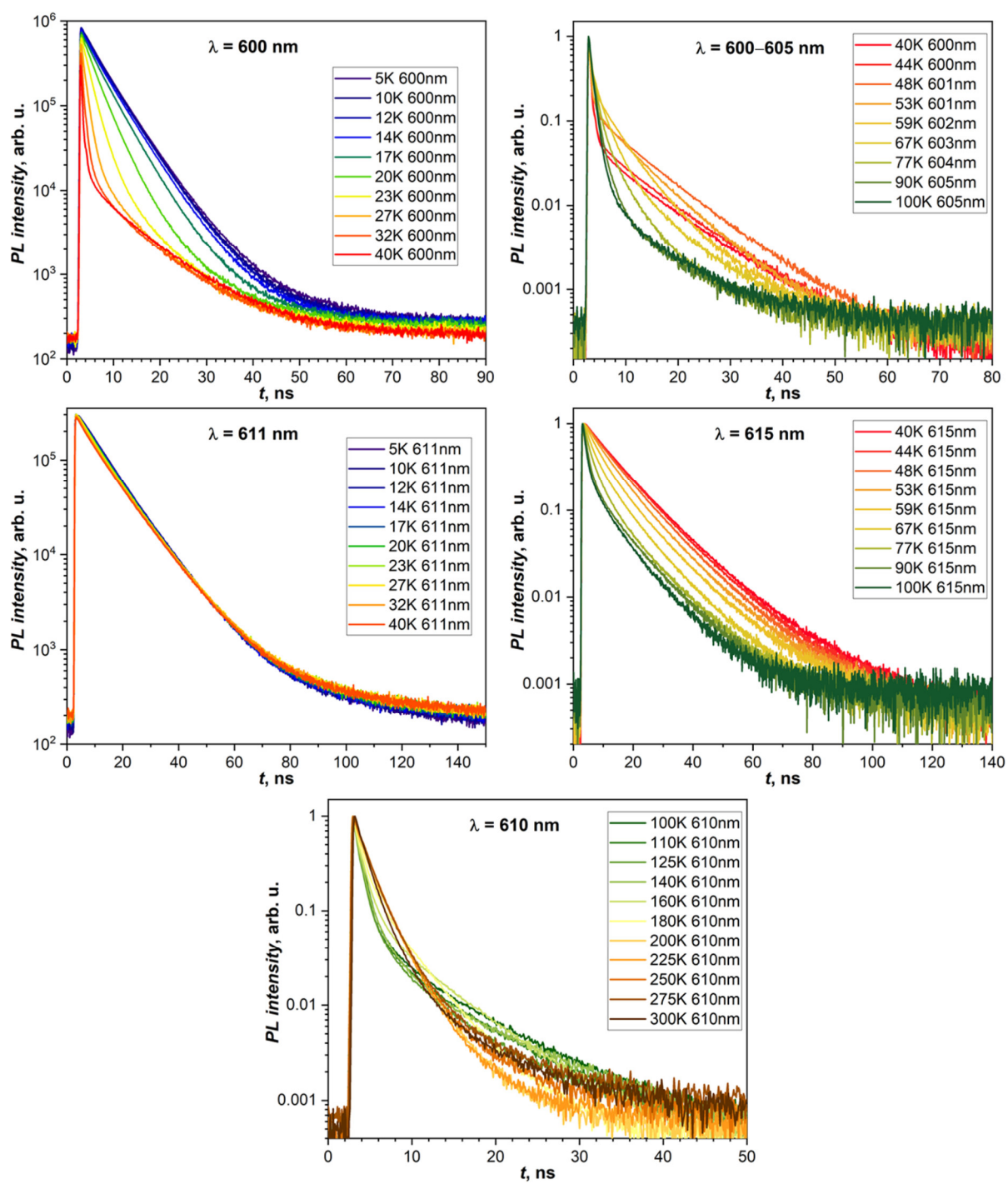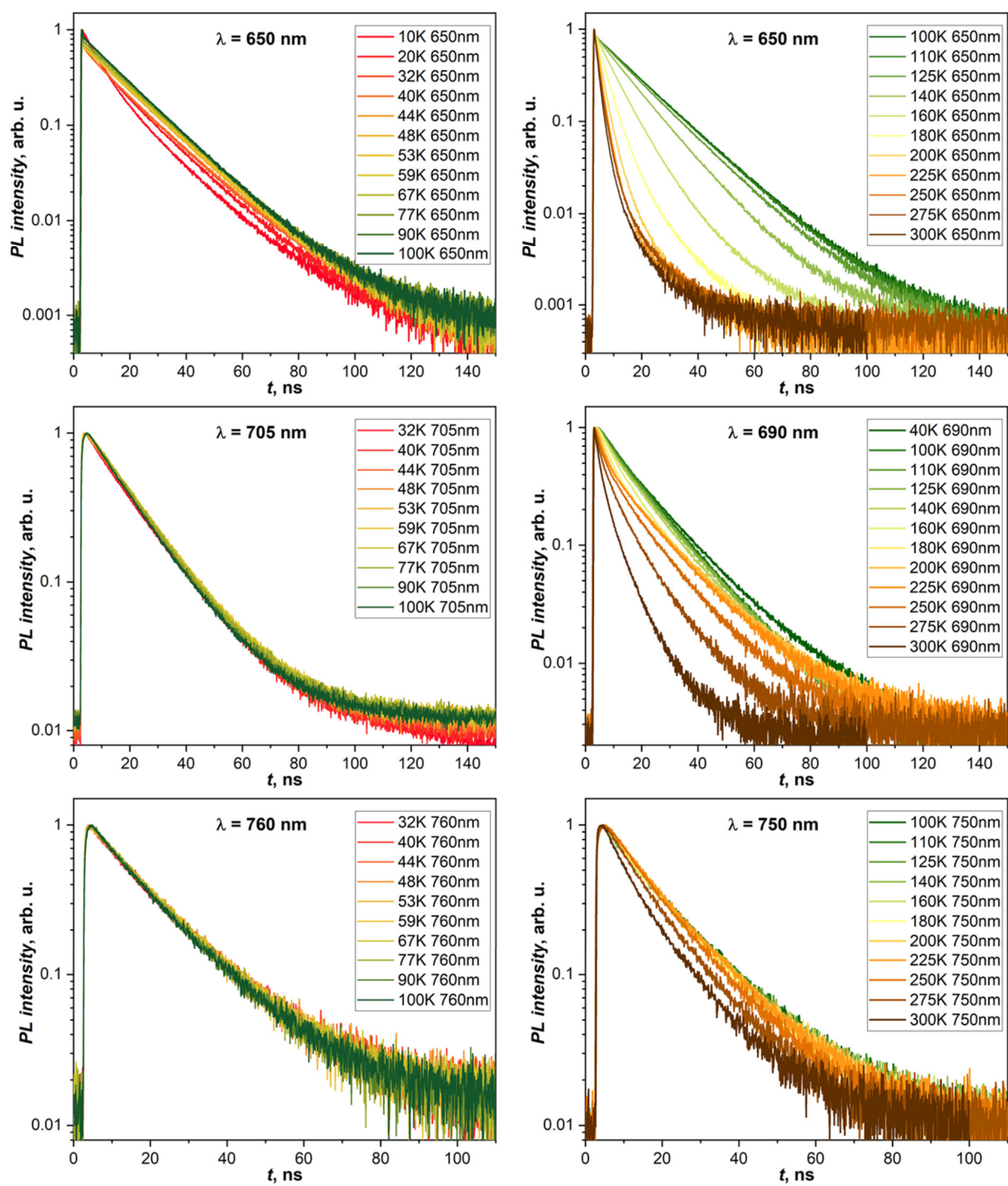| $T$, K | $\lambda$, nm | $\tau_1$, ns | $\pm\Delta\tau_1$, ns | $W_1$, % | $\tau_2$, ns | $\pm\Delta\tau_2$, ns | $W_2$, % | $\tau_3$, ns | $\pm\Delta\tau_3$, ns | $W_3$, % |
|---|---|---|---|---|---|---|---|---|---|---|
| 5 | 600 | 3.75 | 0.16 | 48 | 6.10 | 0.10 | 51 | 58.0 | 1.4 | 01 |
| 10 | 600 | 3.79 | 0.14 | 52 | 6.07 | 0.11 | 47 | 65.0 | 2.0 | 01 |
| 12 | 600 | 3.64 | 0.16 | 46 | 5.86 | 0.09 | 54 | 69.2 | 2.4 | 01 |
| 14 | 600 | 3.69 | 0.16 | 48 | 5.78 | 0.10 | 51 | 78.3 | 3.3 | 01 |
| 17 | 600 | 3.81 | 0.06 | 80 | 6.43 | 0.18 | 20 | 77.9 | 3.8 | 01 |
| 20 | 600 | 2.96 | 0.02 | 89 | 7.40 | 0.13 | 11 | 71.9 | 4.2 | 01 |
| 23 | 600 | 1.91 | 0.02 | 86 | 7.49 | 0.08 | 13 | 47.0 | 2.3 | 01 |
| 27 | 600 | 1.08 | 0.01 | 78 | 7.42 | 0.08 | 20 | 28.7 | 1.3 | 02 |
| 32 | 600 | 0.67 | 0.01 | 63 | 7.43 | 0.12 | 31 | 19.8 | 0.8 | 06 |
| 40 | 600 | 0.48 | 0.01 | 40 | 7.46 | 0.22 | 42 | 15.0 | 0.6 | 18 |
| | | | | | | | | | | |
| 40 | 600 | 0.48 | 0.01 | 41 | 8.63 | 0.15 | 52 | 19.9 | 1.2 | 08 |
| 44 | 600 | 0.43 | 0.01 | 33 | 8.27 | 0.19 | 55 | 16.6 | 1.0 | 12 |
| 48 | 601 | 0.45 | 0.02 | 19 | 8.56 | 0.07 | 77 | 24.0 | 2.0 | 04 |
| 53 | 601 | 0.38 | 0.02 | 19 | 6.79 | 0.07 | 75 | 17.7 | 1.0 | 06 |
| 59 | 602 | 0.41 | 0.03 | 15 | 4.52 | 0.05 | 74 | 13.4 | 0.3 | 11 |
| 67 | 603 | 1.63 | 0.04 | 62 | 5.34 | 0.24 | 31 | 14.4 | 0.8 | 07 |
| 77 | 604 | 0.88 | 0.03 | 57 | 3.50 | 0.09 | 36 | 12.1 | 0.5 | 07 |
| 90 | 605 | 0.78 | 0.03 | 68 | 2.30 | 0.12 | 22 | 11.0 | 0.3 | 10 |
| 100 | 605 | 0.74 | 0.02 | 76 | 2.78 | 0.25 | 12 | 10.7 | 0.3 | 12 |
| | | | | | | | | | | |
| 100 | 610 | 0.87 | 0.02 | 60 | 4.56 | 0.25 | 21 | 11.59 | 0.31 | 19 |
| 110 | 610 | 0.77 | 0.02 | 58 | 3.64 | 0.21 | 22 | 10.05 | 0.24 | 21 |
| 125 | 610 | 0.80 | 0.02 | 60 | 3.95 | 0.14 | 28 | 12.28 | 0.45 | 12 |
| 140 | 610 | 0.79 | 0.03 | 51 | 2.68 | 0.11 | 28 | 11.24 | 0.15 | 21 |
| 160 | 610 | 1.02 | 0.02 | 56 | 5.27 | 0.34 | 31 | 9.27 | 0.85 | 13 |
| 180 | 610 | 0.94 | 0.03 | 41 | 3.57 | 0.07 | 54 | 9.17 | 0.72 | 05 |
| 200 | 610 | 1.17 | 0.07 | 35 | 2.69 | 0.06 | 62 | 10.25 | 0.73 | 03 |
| 225 | 610 | 1.94 | 0.02 | 92 | 5.96 | 0.16 | 08 | | | |
| 250 | 610 | 1.95 | 0.01 | 91 | 7.64 | 0.17 | 09 | | | |
| 275 | 610 | 1.87 | 0.01 | 89 | 7.79 | 0.14 | 11 | | | |
| 300 | 610 | 1.54 | 0.01 | 87 | 6.88 | 0.10 | 13 | | | |
| | | | | | | | | | | |
| 300 | 610 nm 0 T | 1.54 | 0.01 | 87 | 6.88 | 0.10 | 13 | | | |
| 300 | 610 nm 0.03 T | 1.48 | 0.01 | 88 | 6.61 | 0.11 | 12 | | | |
| 300 | 610 nm 0.3 T | 1.63 | 0.01 | 85 | 7.34 | 0.10 | 15 | | | |
| 300 | 610 nm 1.5 T | 1.63 | 0.01 | 85 | 7.35 | 0.10 | 15 | | | |

$\pm\Delta\tau_i$ is a standard deviation of $\tau_i$ from exponential fit; $W_i$ – weight of the given $\tau_i$, ($W_1 + W_2 + W_3$ = 100%)

**Table S1b.** Multiexponential fitting of PL decay curves at 611–615 nm (dominant state II)

| *T*, K | λ, nm | τ$_1$, ns | ±Δτ$_1$, ns | W$_1$, % | τ$_2$, ns | ±Δτ$_2$, ns | W$_2$, % |
|---|---|---|---|---|---|---|---|
| 5 | 611 | **9.86** | 0.03 | 97 | **34.7** | 0.6 | 03 |
| 10 | 611 | **9.93** | 0.02 | 97 | **34.2** | 0.6 | 03 |
| 12 | 611 | **9.92** | 0.03 | 97 | **34.0** | 0.7 | 03 |
| 14 | 611 | **9.92** | 0.02 | 97 | **33.7** | 0.7 | 03 |
| 17 | 611 | **9.90** | 0.03 | 97 | **32.2** | 0.6 | 03 |
| 20 | 611 | **9.95** | 0.03 | 97 | **32.0** | 0.6 | 03 |
| 23 | 611 | **9.92** | 0.03 | 96 | **29.9** | 0.5 | 04 |
| 27 | 611 | **9.99** | 0.03 | 96 | **29.3** | 0.5 | 04 |
| 32 | 611 | **10.09** | 0.03 | 95 | **29.1** | 0.5 | 05 |
| 40 | 611 | **10.16** | 0.03 | 96 | **30.2** | 0.6 | 04 |
|  |  |  |  |  |  |  |  |
| 40 | 615 | **10.82** | 0.06 | 89 | **25.18** | 0.44 | 11 |
| 44 | 615 | **10.69** | 0.06 | 91 | **25.28** | 0.53 | 09 |
| 48 | 615 | **10.21** | 0.06 | 91 | **24.74** | 0.52 | 09 |
| 53 | 615 | **9.12** | 0.06 | 86 | **21.31** | 0.34 | 14 |
| 59 | 615 | **7.30** | 0.08 | 72 | **16.80** | 0.17 | 28 |
| 67 | 615 | **5.64** | 0.08 | 62 | **13.95** | 0.11 | 38 |
| 77 | 615 | **3.75** | 0.06 | 57 | **13.12** | 0.07 | 43 |
| 90 | 615 | **2.04** | 0.04 | 43 | **11.61** | 0.05 | 57 |
| 100 | 615 | **2.09** | 0.05 | 40 | **10.56** | 0.05 | 60 |

±Δτ$_i$ is a standard deviation of τ$_i$ from exponential fit; $W_i$ – weight of the given τ$_i$, ($W_1$ + $W_2$ = 100%)

**Table S1c.** Multiexponential fitting of PL decay curves at 650 nm (dominant state III, overlap with state I)

| $T$, K | $\lambda$, nm | $\tau_1$, ns | $\pm\Delta\tau_1$, ns | $W_1$, % | $\tau_2$, ns | $\pm\Delta\tau_2$, ns | $W_2$, % | $\tau_3$, ns | $\pm\Delta\tau_3$, ns | $W_3$, % |
|---|---|---|---|---|---|---|---|---|---|---|
| 10 | 650 | **5.24** | 0.21 | 33 | **14.30** | 0.40 | 62 | 33.4 | 3.7 | 05 |
| 20 | 650 | **3.65** | 0.21 | 15 | **14.47** | 0.21 | 79 | 33.9 | 2.8 | 06 |
| 27 | 650 | **1.18** | 0.16 | 03 | **14.71** | 0.13 | 90 | 32.6 | 2.2 | 07 |
| 32 | 650 | **1.14** | 0.10 | 03 | **14.58** | 0.07 | 89 | 38.3 | 1.3 | 08 |
| 40 | 650 | **0.52** | 0.06 | 01 | **14.60** | 0.08 | 90 | 35.4 | 1.1 | 09 |
| | | | | | | | | | | |
| 40 | 650 | **0.26** | 0.07 | 01 | **15.18** | 0.10 | 95 | 37.7 | 3.4 | 04 |
| 44 | 650 | **0.27** | 0.05 | 01 | **15.46** | 0.07 | 97 | 49.7 | 6.4 | 03 |
| 48 | 650 | **0.24** | 0.05 | 00 | **15.50** | 0.08 | 96 | 42.9 | 5.2 | 03 |
| 53 | 650 | **0.22** | 0.04 | 00 | **15.76** | 0.06 | 97 | 79.6 | 18.3 | 02 |
| 59 | 650 | **0.19** | 0.04 | 00 | **15.72** | 0.07 | 97 | 54.3 | 8.5 | 02 |
| 67 | 650 | **0.18** | 0.05 | 00 | **15.66** | 0.08 | 97 | 45.1 | 6.2 | 03 |
| 77 | 650 | **0.20** | 0.06 | 00 | **15.43** | 0.07 | 97 | 44.9 | 6.6 | 03 |
| 90 | 650 | **0.25** | 0.10 | 00 | **15.10** | 0.08 | 96 | 37.5 | 4.0 | 03 |
| 100 | 650 | **0.39** | 0.15 | 00 | **15.02** | 0.08 | 96 | 41.4 | 4.4 | 03 |
| | | | | | | | | | | |
| 100 | 650 | **0.34** | 0.16 | 00 | **14.89** | 0.07 | 95 | 33.6 | 2.1 | 05 |
| 110 | 650 | **0.62** | 0.26 | 01 | **14.86** | 0.07 | 96 | 39.1 | 2.8 | 03 |
| 125 | 650 | **0.97** | 0.30 | 01 | **14.12** | 0.06 | 96 | 39.6 | 2.7 | 03 |
| 140 | 650 | **2.98** | 0.69 | 03 | **11.74** | 0.07 | 94 | 38.7 | 2.1 | 03 |
| 160 | 650 | **6.18** | 0.15 | 67 | **11.08** | 0.61 | 30 | 36.3 | 3.1 | 03 |
| 180 | 650 | **3.65** | 0.04 | 78 | **9.78** | 0.24 | 20 | 43.7 | 4.4 | 02 |
| 200 | 650 | **2.46** | 0.02 | 83 | **7.45** | 0.20 | 15 | 38.7 | 3.3 | 02 |
| 225 | 650 | **1.96** | 0.03 | 80 | **4.98** | 0.25 | 15 | 20.5 | 0.8 | 04 |
| 250 | 650 | **1.93** | 0.02 | 82 | **6.41** | 0.31 | 14 | 22.7 | 1.3 | 04 |
| 275 | 650 | **1.84** | 0.02 | 80 | **7.13** | 0.17 | 17 | 45.1 | 5.1 | 03 |
| 300 | 650 | **1.40** | 0.02 | 74 | **4.22** | 0.15 | 21 | 16.8 | 1.2 | 05 |

$\pm\Delta\tau_i$ is a standard deviation of $\tau_i$ from exponential fit; $W_i$ – weight of the given $\tau_i$, ($W_1 + W_2 + W_3 = 100\%$)

**Table S1d.** Multiexponential fitting of PL decay curves at 690-705 nm (state IV, overlap with state III)

| $T$, K | $\lambda$, nm | $\tau_1$, ns | $\pm\Delta\tau_1$, ns | $W_1$, % | $\tau_2$, ns | $\pm\Delta\tau_2$, ns | $W_2$, % |
|---|---|---|---|---|---|---|---|
| 40 | 705 | **15.71** | 0.12 | 96 | **51.7** | 11.1 | 04 |
| 44 | 705 | **15.67** | 0.16 | 95 | **38.9** | 7.1 | 05 |
| 48 | 705 | **15.98** | 0.12 | 97 | **56.3** | 18.7 | 03 |
| 53 | 705 | **16.12** | 0.08 | 97 | **122.5** | 86.2 | 03 |
| 59 | 705 | **15.98** | 0.10 | 97 | **65.6** | 22.3 | 03 |
| 67 | 705 | **15.74** | 0.14 | 96 | **41.0** | 8.9 | 04 |
| 77 | 705 | **15.39** | 0.14 | 96 | **38.8** | 7.5 | 04 |
| 90 | 705 | **14.86** | 0.14 | 95 | **35.6** | 4.9 | 05 |
| 100 | 705 | **14.88** | 0.13 | 95 | **38.4** | 5.8 | 05 |
| | | | | | | | |
| 100 | 690 | **12.87** | 0.19 | 78 | **23.6** | 0.8 | 21 |
| 110 | 690 | **12.42** | 0.18 | 76 | **23.5** | 0.7 | 24 |
| 125 | 690 | **12.13** | 0.18 | 72 | **23.4** | 0.6 | 28 |
| 140 | 690 | **12.01** | 0.12 | 80 | **27.3** | 0.7 | 19 |
| 160 | 690 | **8.98** | 0.09 | 62 | **23.6** | 0.2 | 37 |
| 180 | 690 | **5.87** | 0.08 | 40 | **20.5** | 0.1 | 60 |
| 200 | 690 | **4.98** | 0.10 | 29 | **19.2** | 0.1 | 71 |
| 225 | 690 | **5.70** | 0.14 | 28 | **18.2** | 0.1 | 72 |
| 250 | 690 | **5.46** | 0.13 | 33 | **16.2** | 0.1 | 67 |
| 275 | 690 | **4.48** | 0.10 | 43 | **13.2** | 0.1 | 57 |
| 300 | 690 | **2.50** | 0.04 | 47 | **8.3** | 0.1 | 53 |

$\pm\Delta\tau_i$ is a standard deviation of $\tau_i$ from exponential fit; $W_i$ – weight of the given $\tau_i$, ($W_1 + W_2 = 100\%$)

**Table S1e.** Multiexponential fitting of PL decay curves at 750-760 nm (state III, IV, V)

| $T$, K | $\lambda$, nm | $\tau_1$, ns | $\pm\Delta\tau_1$, ns | $W_1$, % | $\tau_2$, ns | $\pm\Delta\tau_2$, ns | $W_2$, % |
|---|---|---|---|---|---|---|---|
| 40 | 760 | **13.38** | 0.91 | 68 | **23.5** | 3.1 | 32 |
| 44 | 760 | **14.78** | 0.45 | 87 | **33.3** | 7.9 | 13 |
| 48 | 760 | **14.48** | 0.68 | 83 | **27.4** | 6.4 | 17 |
| 53 | 760 | **14.61** | 0.60 | 85 | **28.5** | 6.8 | 15 |
| 59 | 760 | **13.96** | 0.95 | 74 | **23.6** | 4.5 | 26 |
| 67 | 760 | **13.95** | 0.65 | 79 | **25.9** | 4.7 | 21 |
| 77 | 760 | **11.84** | 1.21 | 48 | **19.7** | 1.7 | 52 |
| 90 | 760 | **10.66** | 1.04 | 39 | **19.2** | 1.1 | 61 |
| 100 | 760 | **10.20** | 1.05 | 35 | **18.7** | 0.9 | 65 |
|  |  |  |  |  |  |  |  |
| 100 | 750 | **9.07** | 0.65 | 29 | **18.3** | 0.4 | 71 |
| 110 | 750 | **10.22** | 0.59 | 41 | **19.5** | 0.7 | 59 |
| 125 | 750 | **9.80** | 0.53 | 38 | **19.8** | 0.6 | 62 |
| 140 | 750 | **11.71** | 0.42 | 65 | **24.4** | 1.7 | 35 |
| 160 | 750 | **10.15** | 0.35 | 51 | **20.9** | 0.7 | 49 |
| 180 | 750 | **8.69** | 0.39 | 35 | **18.7** | 0.4 | 65 |
| 200 | 750 | **9.94** | 0.49 | 43 | **19.3** | 0.7 | 57 |
| 225 | 750 | **12.42** | 0.32 | 80 | **26.8** | 3.2 | 20 |
| 250 | 750 | **11.03** | 0.47 | 70 | **20.0** | 2.0 | 30 |
| 275 | 750 | **8.86** | 0.53 | 54 | **16.0** | 1.0 | 46 |
| 300 | 750 | **5.57** | 0.26 | 35 | **13.64** | 0.33 | 65 |

$\pm\Delta\tau_i$ is a standard deviation of $\tau_i$ from exponential fit; $W_i$ – weight of the given $\tau_i$, ($W_1 + W_2 = 100\%$)
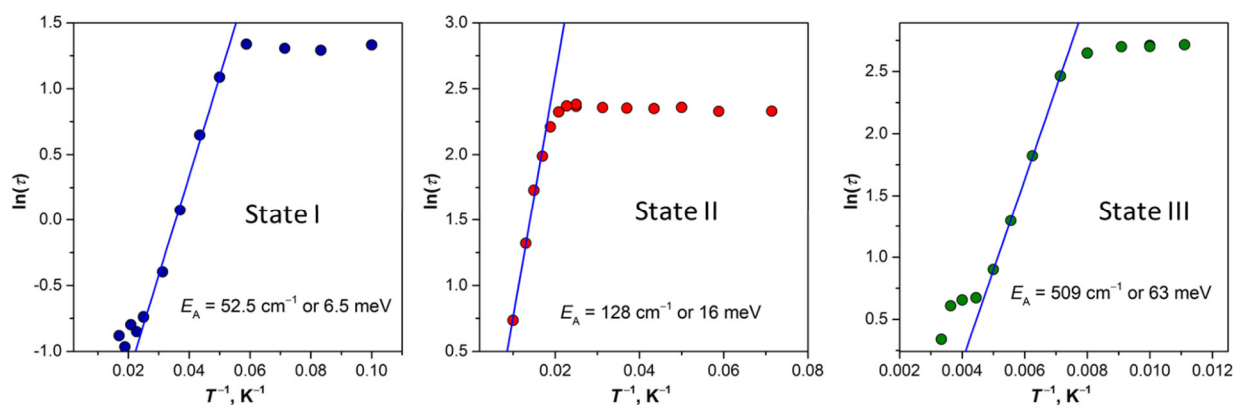
**Figure S7.** PL decay time of states I–III plotted in Arrhenius coordinates, and determination of activation barriers from linear parts.
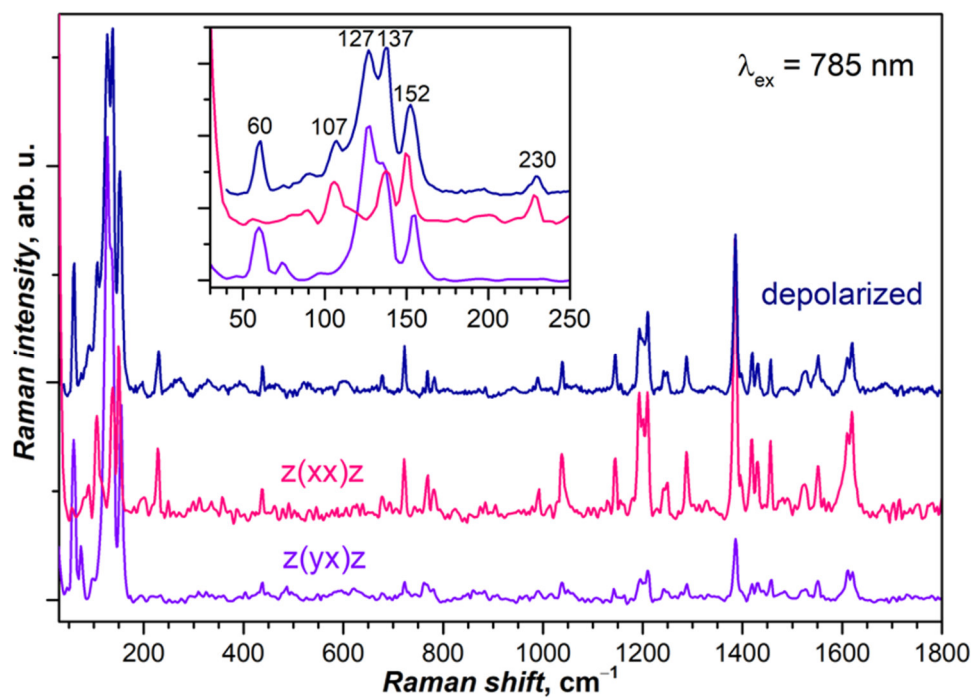


**Figure S8.** Raman spectra of DBP single crystal measured at room temperature with excitation at 785 nm. The inset shows enhancement of the low-frequency range.
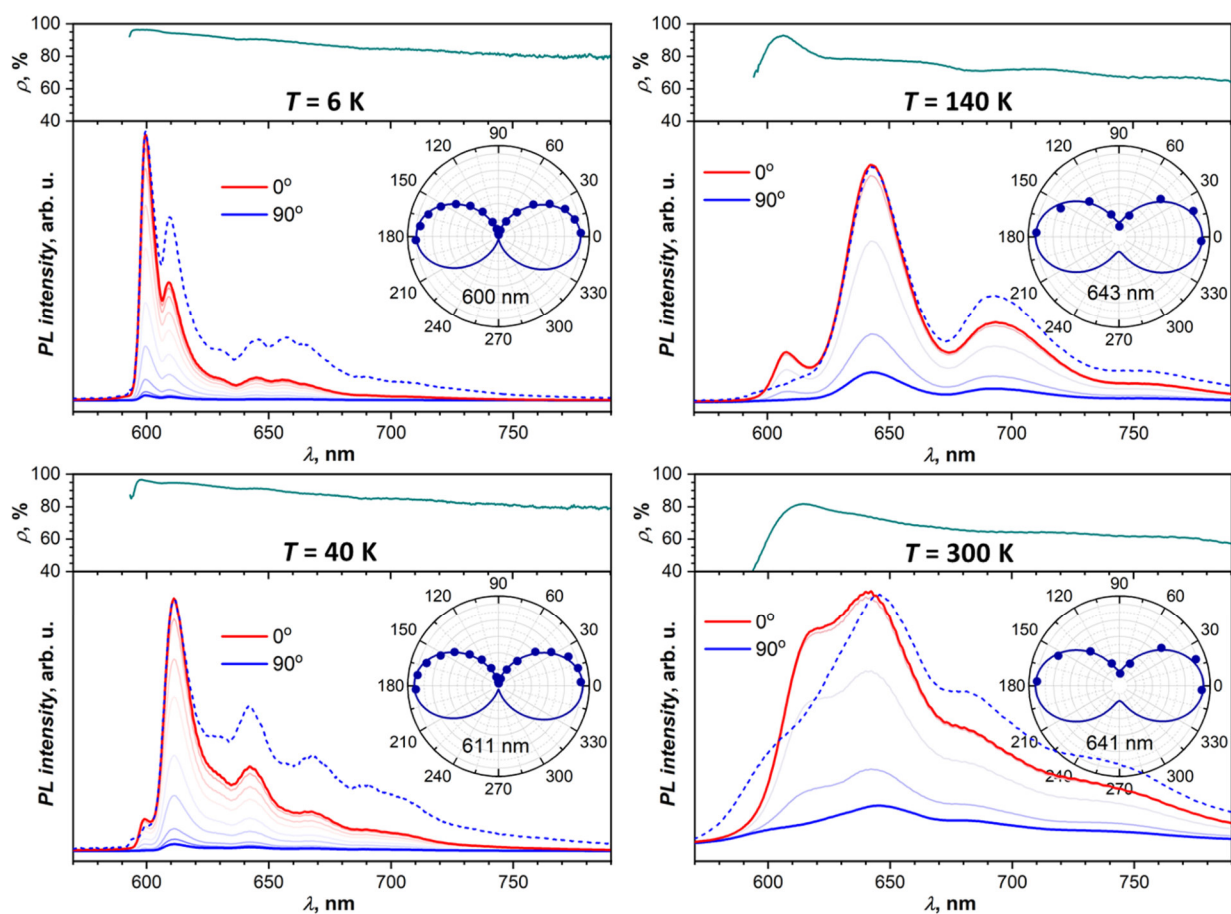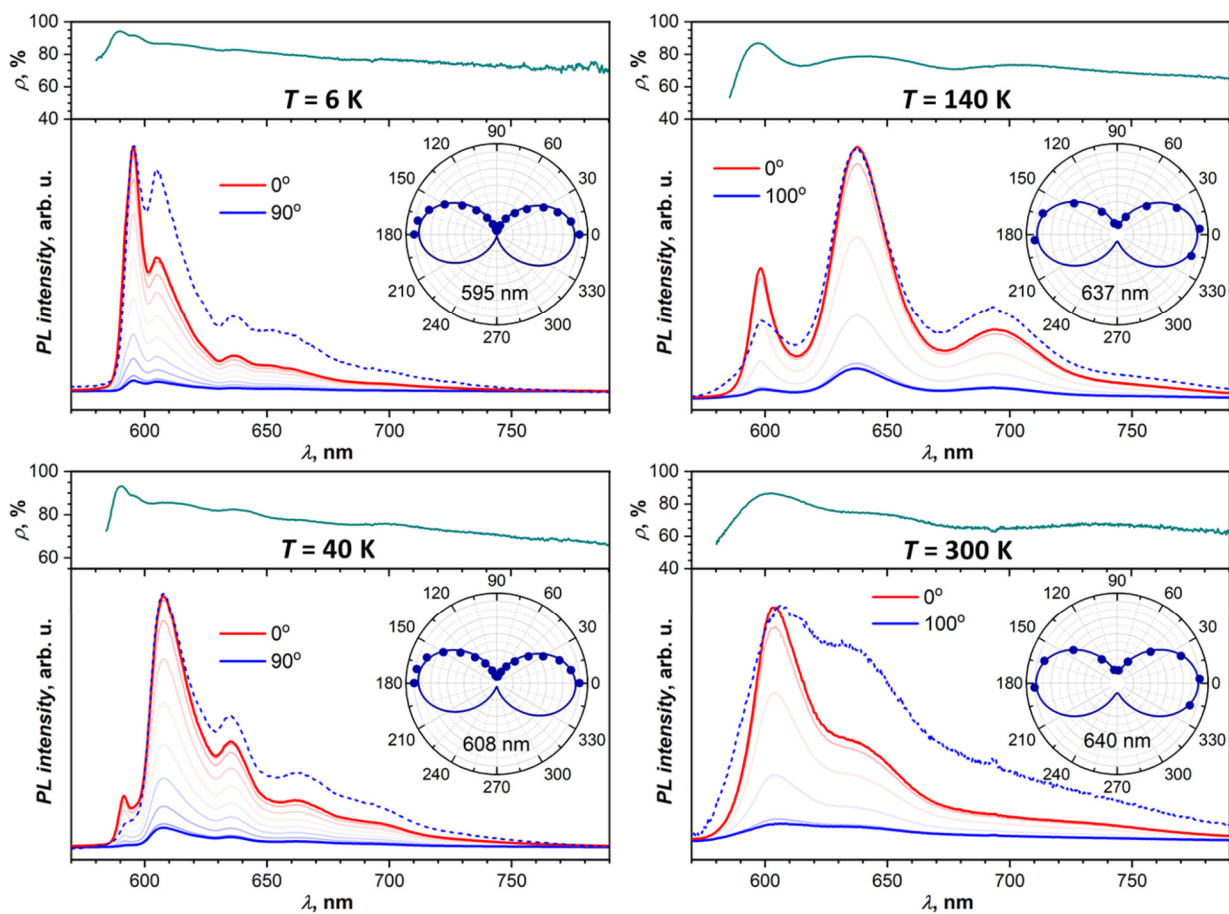
**Polarization dependence of PL**



**Figure S9a.** Polarization angle dependence of DBP single-crystal photoluminescence intensity at different temperatures. Dashed blue lines are spectra measured at 90° (polarization plane parallel to *c*.) and scaled to match intensity of the spectra at 0° (polarization plane parallel to *a*). In addition to spectra measured at different angles, each panel shows polarization ratio $\rho = (I_0 - I_{90})/(I_0 + I_{90})$ at different wavelengths (dark cyan curves) and dependence of the PL intensity on the angle at an indicated wavelength (polar plot insets).

**Figure S9b.** Polarization angle dependence of DBP single-crystal photoluminescence intensity at different temperatures, measurements for a different crystal as in Fig. S9a. Dashed blue lines are spectra measured at 90° (polarization plane parallel to *c*.) and scaled to match intensity of the spectra at 0° (polarization plane parallel to *a*). In addition to spectra measured at different angles, each panel shows polarization ratio $\rho = (I_0 - I_{90})/(I_0 + I_{90})$ at different wavelengths (dark cyan curves) and dependence of the PL intensity on the angle at an indicated wavelength (polar plot insets).

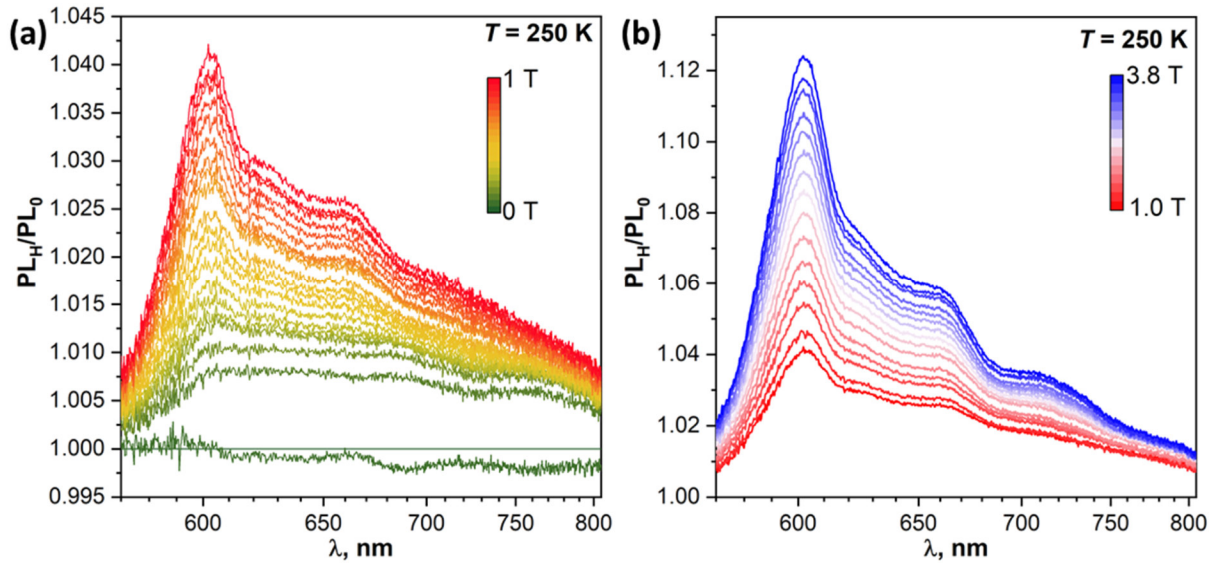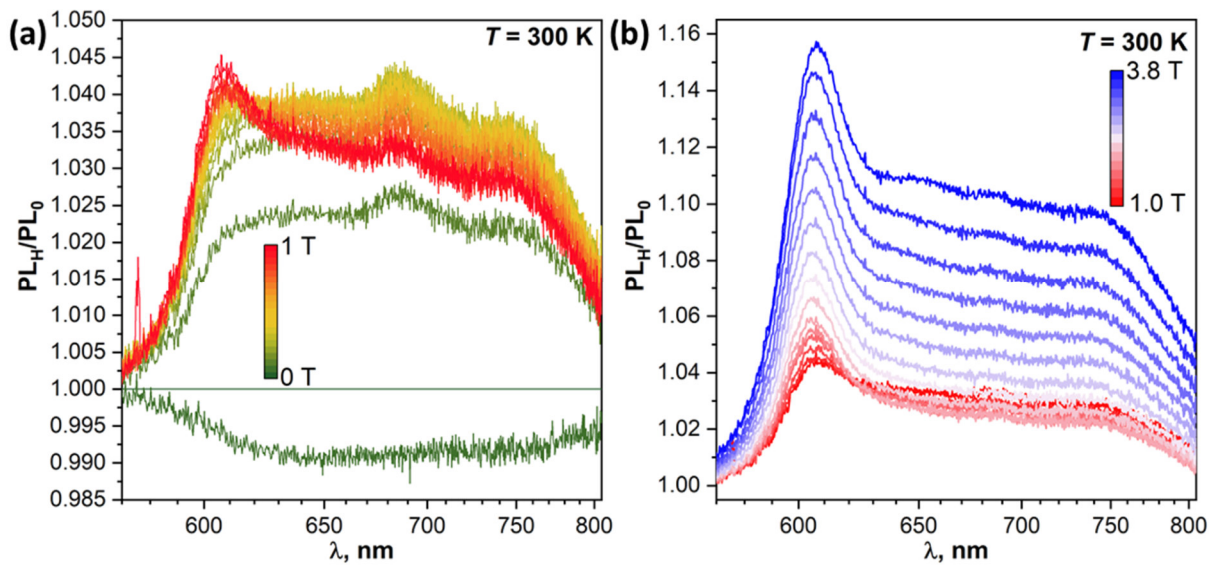**Magneto-PL measurements**
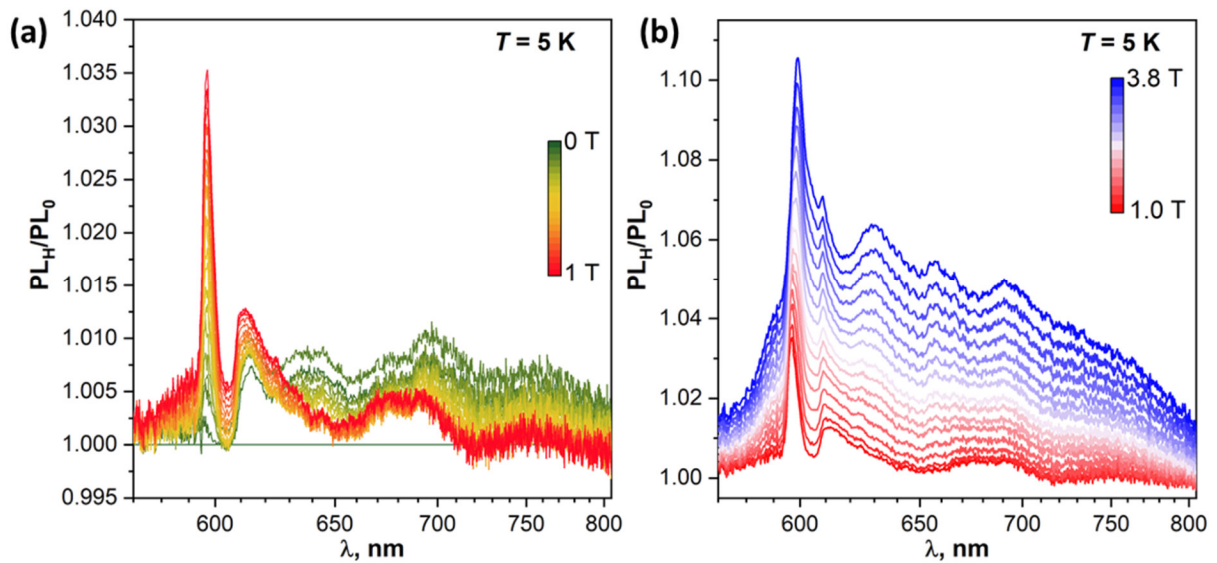


**Figure S10a**. $PL_H/PL_0$ spectra at 5 K in the magnetic field range of: (a) 0−1 T plotted at each 0.05 T; (b) 1−3.8 T plotted at each 0.2 T.
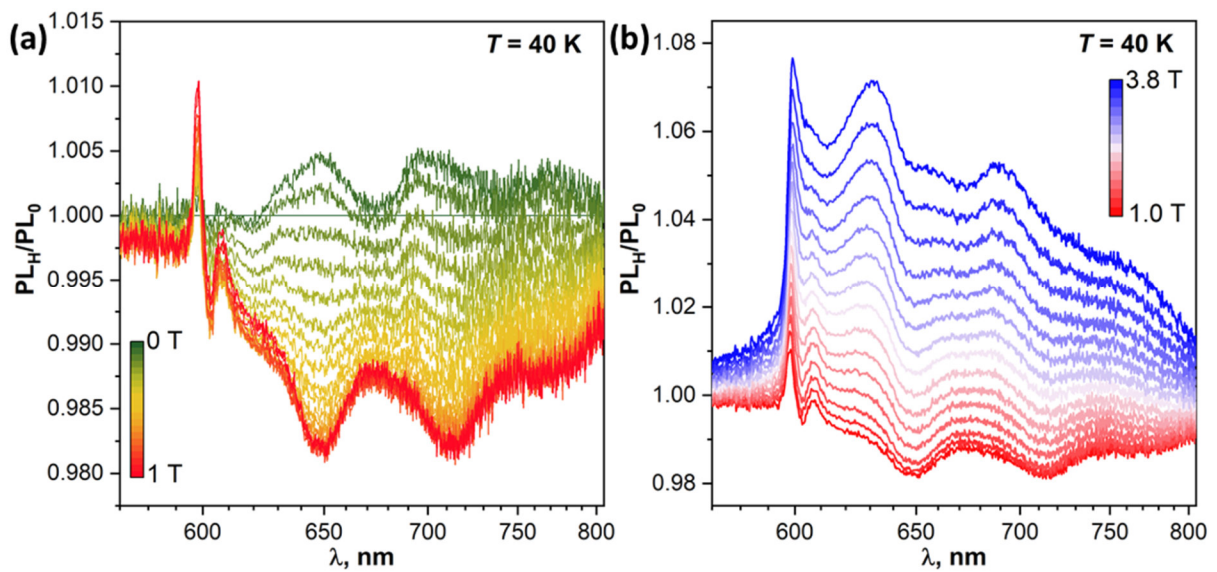


**Figure S10b**. $PL_H/PL_0$ spectra at 40 K in the magnetic field range of: (a) 0−1 T plotted at each 0.05 T; (b) 1−3.8 T plotted at each 0.2 T.
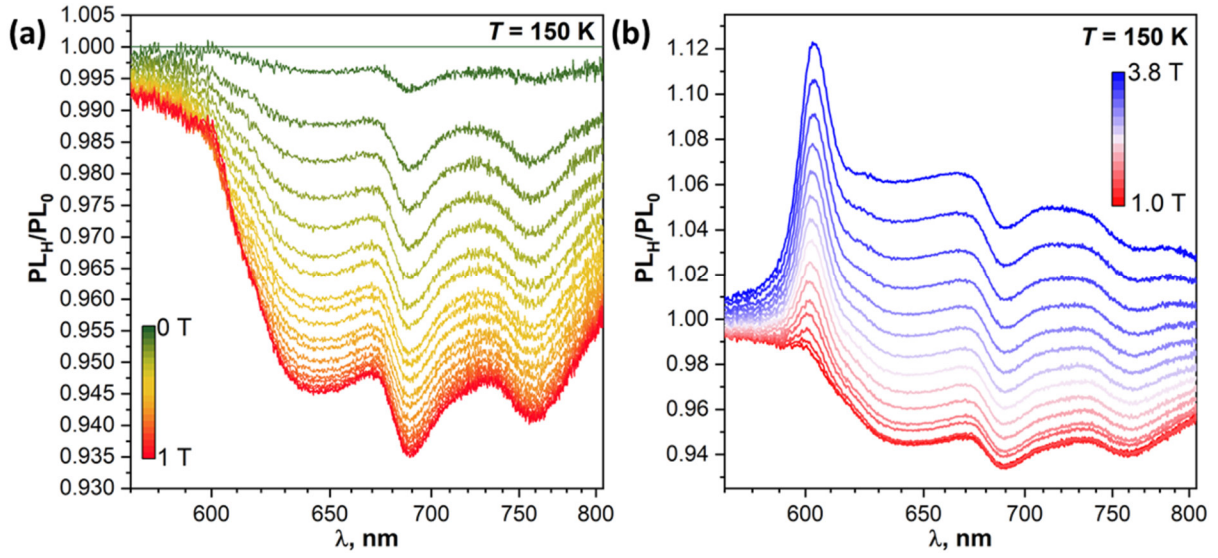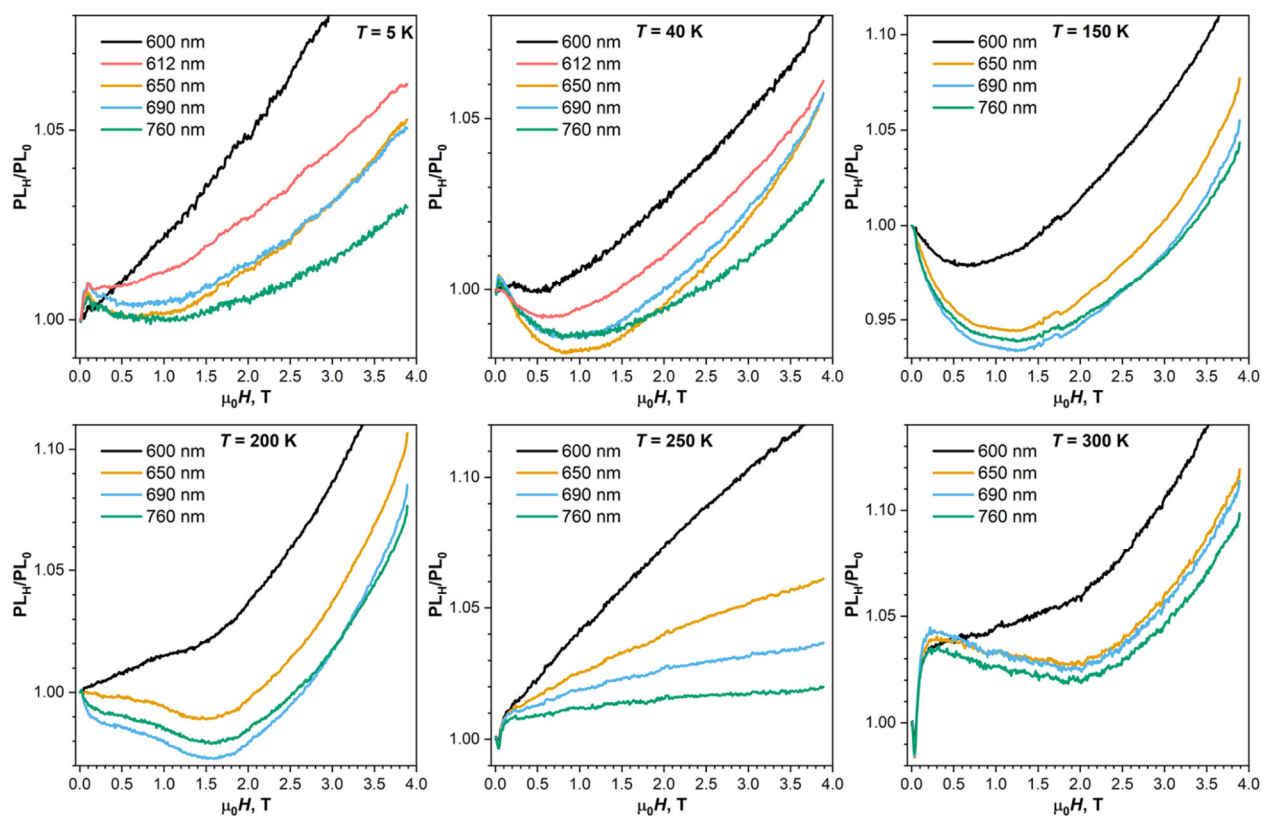
**Figure S10c**. $PL_H/PL_0$ spectra at 150 K in the magnetic field range of: (a) 0−1 T plotted at each 0.05 T; (b) 1−3.8 T plotted at each 0.2 T.
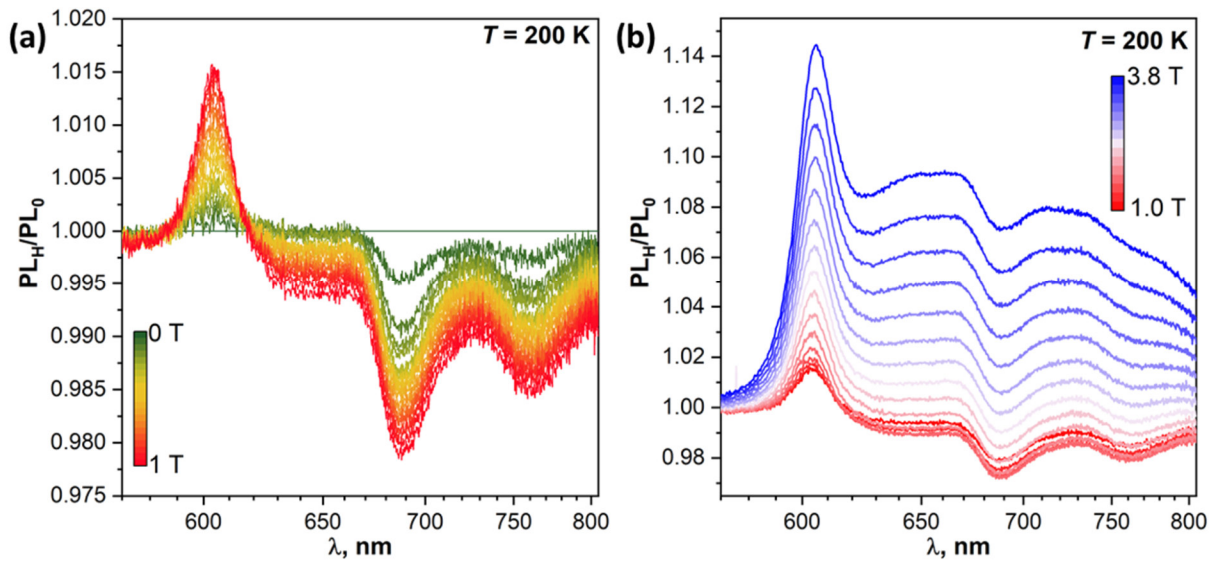


**Figure S10d**. $PL_H/PL_0$ spectra at 200 K in the magnetic field range of: (a) 0−1 T plotted at each 0.05 T; (b) 1−3.8 T plotted at each 0.2 T.

**Figure S10e**. $PL_H/PL_0$ spectra at 250 K in the magnetic field range of: (a) 0−1 T plotted at each 0.05 T; (b) 1−3.8 T plotted at each 0.2 T.



**Figure S10f**. $PL_H/PL_0$ spectra at 300 K in the magnetic field range of: (a) 0−1 T plotted at each 0.05 T; (b) 1−3.8 T plotted at each 0.2 T.

**Figure S11.** Effect of magnetic field on PL intensity at selected temperatures and wavelengths.
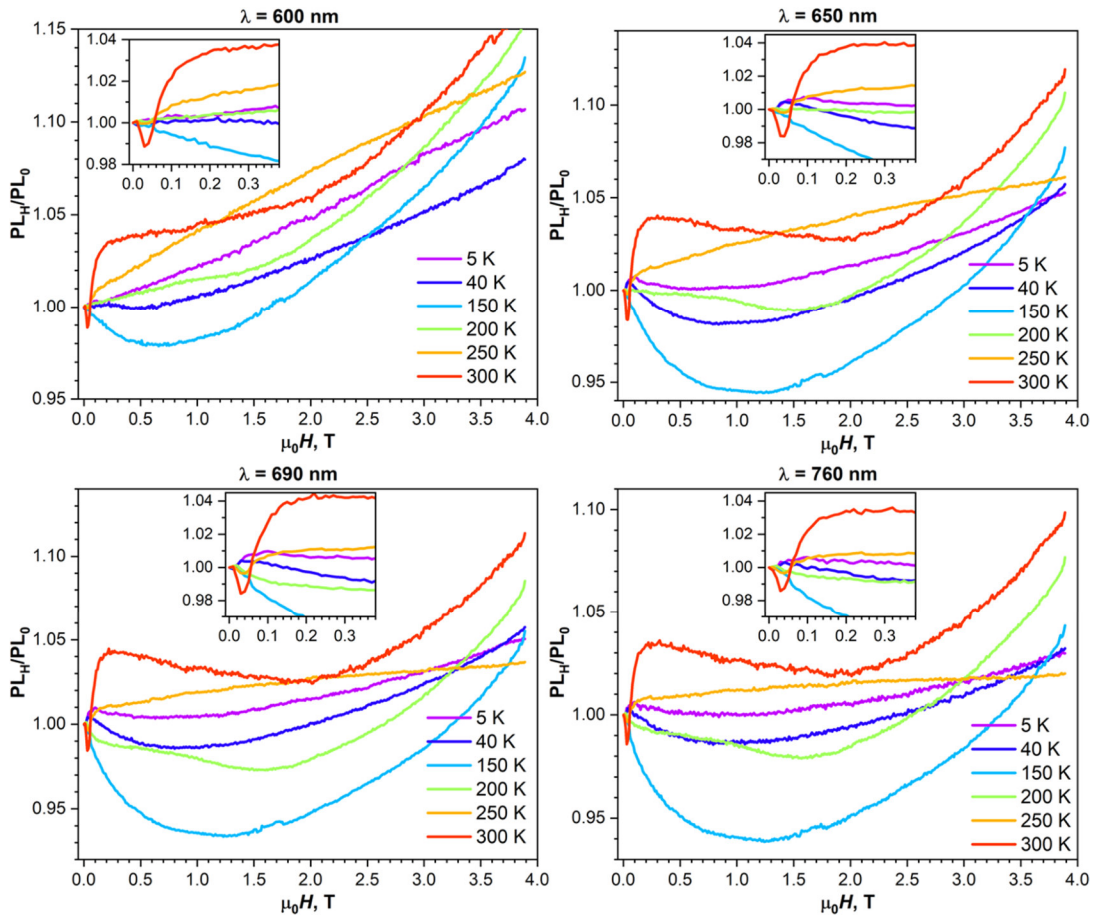
**Figure S12a.** Effect of magnetic field on PL intensity at selected temperatures and wavelengths.
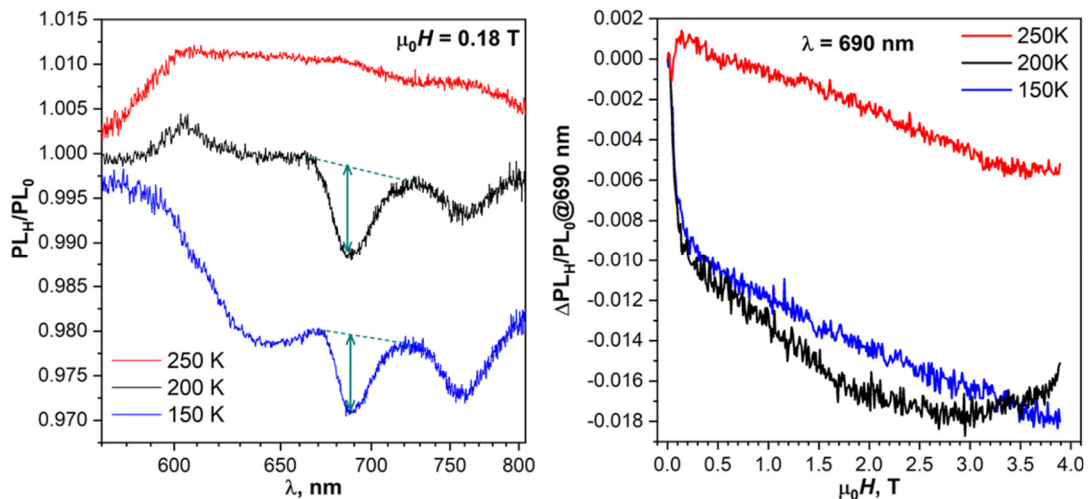


**Figure S12b**. $PL_H/PL_0$ spectra in the magnetic field of 0.18 T highlighting negative peak at 690 nm (left), arrows define $\Delta PL_H/PL_0$ plotted in the right figure as a function of magnetic field. Note the fast decrease of $\Delta PL_H/PL_0$ in small field at 150 and 200 K. Thus, the negative peaks at 690 nm develop during first 0.15–0.20 T, and then change to a more gradual variation with the field.
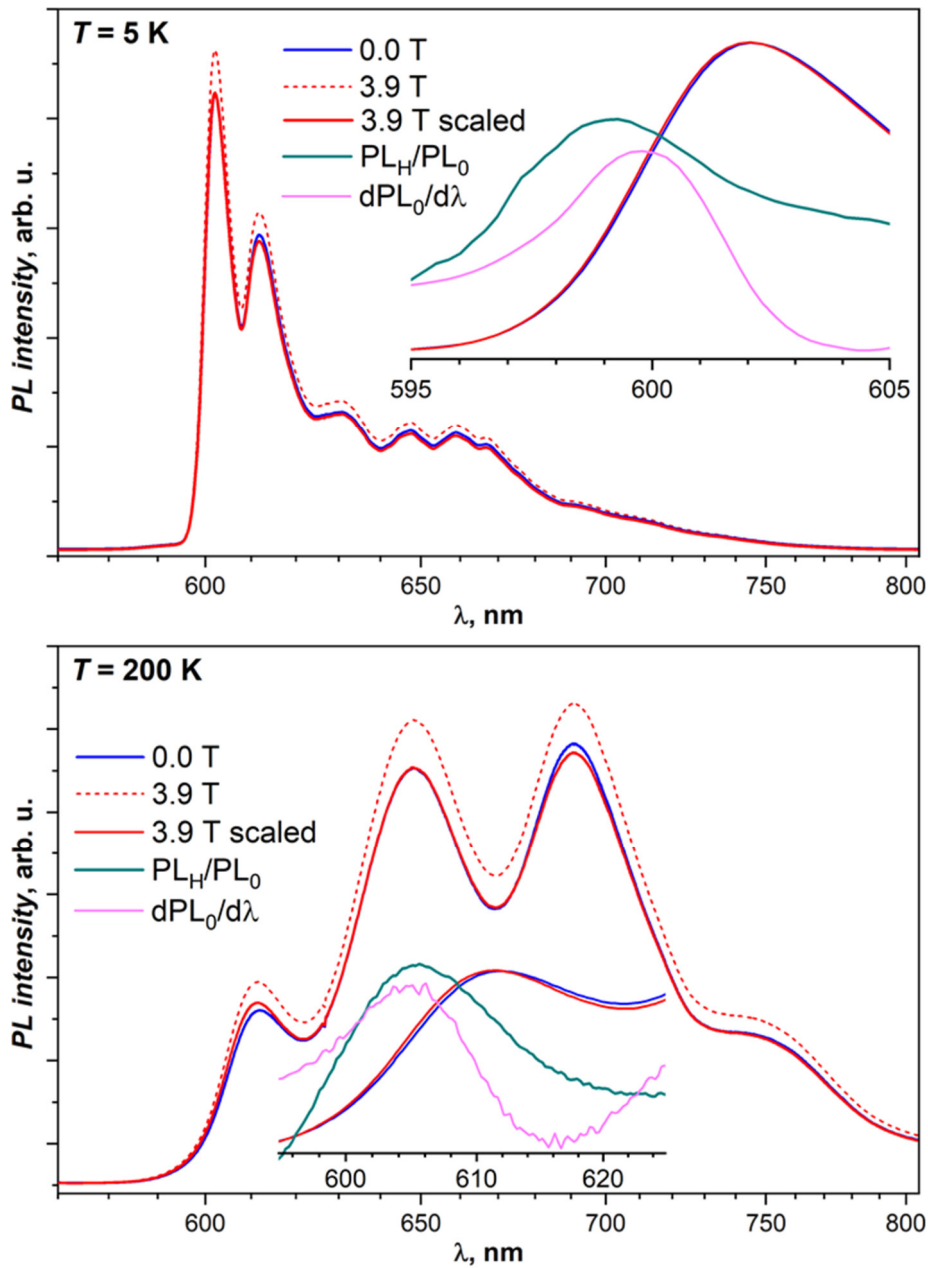
**Figure S13.** Comparison of PL spectra in zero field (blue) and in the field of 3.9 T (red), dashed red line is the 3.9 T spectrum in the actual scale, while solid red line is the spectrum scaled to match intensity of one of the bands in zero-field spectrum. Thus, comparison of blue and solid red curves highlights if some bands show different variation with magnetic field. Importantly, if two overlapping bands show different field dependence, their apparent positions will shift slightly with the field. Insets enlarge the region of the lowest-energy transition near 600 nm showing an apparent shift of the peak in the wavelengths scale, which results in the shift of the $PL_H/PL_0$ maximum from the PL peak position closer to the maximum of PL derivative ($dPL_0/d\lambda$).
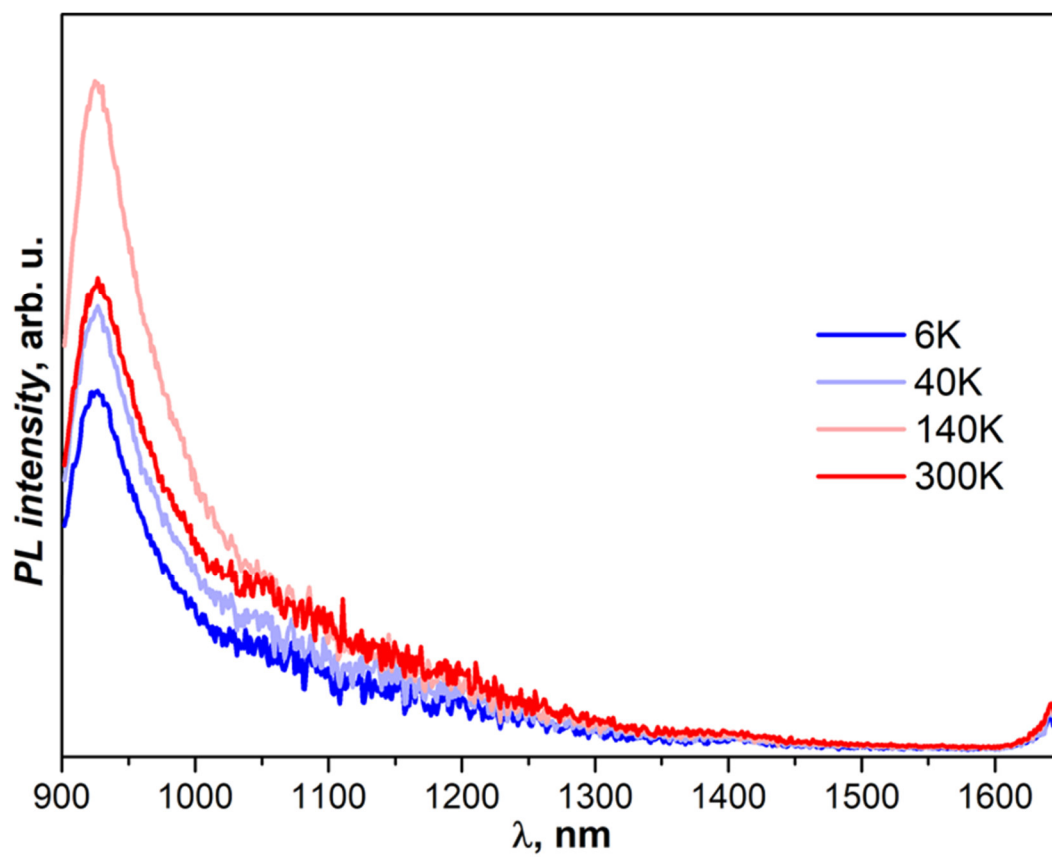
**Figure S14.** NIR-PL measurement of DBP single crystal, excitation with 405 nm laser, emission is passed through 900 nm bandpass filter to Kymera 328i spectrograph and detected with Andor iDus 1.7 μm InGaAs camera. The "peak" at 930 nm in all spectra is caused by the filter cutting strong emission in the visible range.